

Photon temporal modes: a complete framework for quantum information science

B. Brecht^{1*}, Dileep V. Reddy², C. Silberhorn¹, and M. G. Raymer².

¹*Integrated Quantum Optics, Applied Physics, University of Paderborn,
Warburger Strasse 100 33098, Paderborn, Germany and*

²*Oregon Center for Optics, Department of Physics,
University of Oregon, Eugene, Oregon 97403, USA*

(Dated: December 3, 2024)

Temporal modes (TMs) of photonic quantum states provide promising bases for quantum information science (QIS), because they intrinsically span a high-dimensional Hilbert space and lend themselves to integration into existing single-mode fiber communication networks. We show that the three main requirements to construct a valid framework for QIS - the controlled generation of resource states, the targeted and highly efficient manipulation of TMs and their efficient detection, can be fulfilled with current technology. We suggest implementations of diverse QIS applications based on those three building blocks.

INTRODUCTION

Quantum information science (QIS) offers means for storing, transmitting and processing information in ways not achievable using classical information technology. Examples for the benefits of QIS are, amongst others, unconditionally secure communication, ultra-precise metrology beyond classical limits and superior computational algorithms. In principle, all of those can be realized with photons, given that three main prerequisites can be met. For the preparation of good signal carriers, appropriate resource states must be efficiently generated with high reliability. The processing of quantum information requires that controlled operations can be implemented. And finally, efficient detection schemes, which enable faithful information readout, have to be available.

Starting from a very general point-of-view, we note that light has four degrees of freedom (DOF), any of which could be used to encode quantum information: these are the helicity and the three components of the momentum vector. In a beam-like geometry these may be stated as polarization, transverse mode profile (encompassing two DOFs), and energy (that is, frequency). From these DOFs, polarization is most widely applied in quantum information processing. The generation of polarization-entangled Bell states [1] as resource states is nowadays an established experimental method. Two orthogonal polarization modes can easily be separated by means of using polarizing beamsplitters, and proper gate operations are readily implemented with linear optical elements such as waveplates and beamsplitters. However, polarization intrinsically spans a mere two-dimensional Hilbert space, and thus cannot exploit the true potential of QIS, which benefits from higher-dimensional Hilbert spaces.

The second DOF, transverse mode profile, has received considerable attention recently, as it has become apparent that the orbital-angular-momentum (OAM) states of light are a useful basis for encoding information [2–4] and can be efficiently sorted with linear optical ele-

ments [5]. They have been used recently to demonstrate, for instance, enhanced security and bitrate in quantum communication [6–8]. Still, the OAM basis has three drawbacks limiting its current value for some QIS applications: first, it is inherently incompatible with existing single-mode fiber networks because information is encoded onto different spatial field distributions; secondly, it is susceptible to medium perturbations such as turbulence, which affects free-space links; and thirdly, the generation of OAM states with a tailored structure, for instance a well-defined number of modes, is as of yet an unsolved problem.

Only recently has the energy (or frequency) DOF of light been recognized as an underutilized resource for QIS. Because frequency and time are conjugate variables, we call a set of overlapping but orthogonal broadband wave-packet modes by the name “temporal modes”. In a coherent-beam-like or single-transverse-mode guided-wave geometry, temporal modes (TMs) form a complete basis for representing an arbitrary state in the energy degree of freedom [9]. TMs overlap in time and frequency, yet are field-orthogonal. In this respect, they are analogous to transverse spatial modes, yet possess distinct advantages. Since all TMs “live” inside the same spatial field distribution, they are naturally suited for use with highly efficient and experimentally robust waveguide devices and existing single-mode fiber networks. In addition, they are insensitive to stationary or slowly-varying medium perturbations such as linear dispersion, due to their overlapping spectra, making them suitable for real-world applications.

The key enabling development for constructing a valid framework for QIS using TMs is the recent discovery of means for sorting TMs with high efficiency and selectivity in excess of 99.5 percent. This “quantum pulse gate” is achieved by multi-stage quantum frequency conversion driven by tailored, time-dependent laser control pulses [10–13].

While the TM concept applies to any states of light (e.g., squeezed-quadrature states [14, 15]), here we focus

on single-photon states. In this context, not only are temporal modes a complete mode set for expanding the electromagnetic field, but they can also be regarded as a complete set of quantum states for a single photon.

Another important connection of TMs to QIS is that photonic quantum memories rely on storing properly shaped single-photon wave packets in electronic states of atomic ensembles [16]. Therefore, the TM framework proposed here will seamlessly interface with quantum communication architectures, which rely on such memories for long-distance entanglement distribution [17].

In this paper, we propose a complete framework for QIS based on TMs of photonic quantum states. We show that all of the needed elements for quantum information processing with single-photon wave packets can be achieved - the controlled generation and full characterization of resource states, the targeted manipulation of TMs, and their efficient detection. We first introduce the basic concepts of our framework by formally defining TMs and their use as an information-encoding basis. Then we briefly review the current state-of-the-art of generating TMs with ultrafast parametric down-conversion and manipulating them with quantum pulse gates. [10–13]. In particular, previous generation methods are shown to not yet be advanced enough to render TMs a useful basis for QIS. We solve this issue by introducing a method for the generation of photon pair entangled states that contain a user-defined and well-controlled number of TMs. In addition, we discuss in detail the implementation of TM quantum-state tomography of single-photon and photon-pair states. Finally, we combine these methods to discuss the implementation of QIS applications based on TMs. We carefully consider different quantum communication and computation applications, including but not limited to high-dimensional quantum key distribution and linear optical quantum computation.

CONCEPTS

Temporal modes for single-photon states

For a fixed polarization and transverse field distribution (e.g. in a beam-like geometry), a single-photon quantum state in a specific temporal mode (TM) can be expressed as a coherent superposition of a continuum of single-photon states in different monochromatic modes:

$$|A_j\rangle = \int \frac{d\omega}{2\pi} f_j(\omega) \hat{a}^\dagger(\omega) |0\rangle. \quad (1)$$

Here, $\hat{a}^\dagger(\omega)$ is the standard monochromatic creation operator and $f_j(\omega)$ is the complex spectral amplitude of the wave-packet. By Fourier transform, this same state can be expressed as a coherent superposition over many

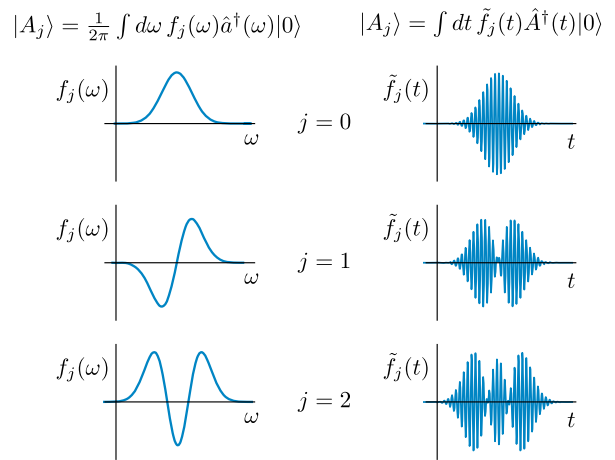


FIG. 1. First three members of a TM basis in the frequency domain (left) and the time domain (right).

possible “creation times”, and then reads

$$|A_j\rangle = \int dt \tilde{f}_j(t) \hat{A}^\dagger(t) |0\rangle \equiv \hat{A}_j^\dagger |0\rangle, \quad (2)$$

where we used the definition

$$\hat{a}^\dagger(\omega) = \int dt e^{i\omega t} \hat{A}^\dagger(t); \quad \hat{A}^\dagger(t) = \int \frac{d\omega}{2\pi} e^{-i\omega t} \hat{a}^\dagger(\omega). \quad (3)$$

In Eq. (2), $\tilde{f}_j(t)$ is the temporal shape of the wave packet (defined as the Fourier transform of $f_j(\omega)$) and $\hat{A}^\dagger(t)$ creates a photon at time t . We also defined a so-called broadband mode operator

$$\hat{A}_j^\dagger = \int dt \tilde{f}_j(t) \hat{A}^\dagger(t) = \frac{1}{2\pi} \int d\omega f_j(\omega) \hat{a}^\dagger(\omega), \quad (4)$$

which creates the wave-packet state $|A_j\rangle$. In Fig. 1, we exemplarily plot the first three members of a TM basis. With this, it is possible to express every single-photon temporal wave-packet quantum state $|\Psi\rangle$ in a basis of TMs as

$$|\Psi\rangle = \sum_{j=0}^{\infty} c_j \hat{A}_j^\dagger |0\rangle, \quad (5)$$

with complex-valued expansion coefficients c_j .

We want to highlight that, although they fully overlap in polarization, space and frequency (time), TMs are orthogonal with respect to a frequency (time) integral

$$\frac{1}{2\pi} \int d\omega f_j^*(\omega) f_k(\omega) = \int dt \tilde{f}_j^*(t) \tilde{f}_k(t) = \delta_{jk}. \quad (6)$$

They also obey bosonic commutation relations [9, 18]

$$[\hat{A}_i^\dagger, \hat{A}_j] = \delta_{ij} \quad (7)$$

just as the well-known monochromatic creation operators.

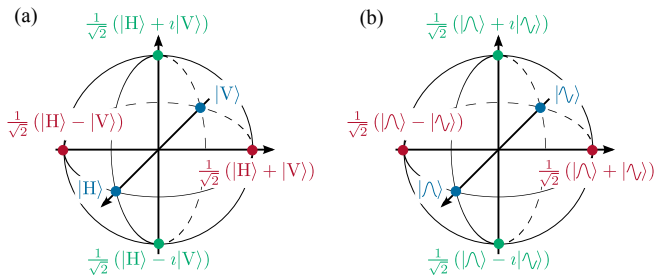


FIG. 2. (a) Poincaré sphere. The logical “0” and “1” of a polarization qubit can be encoded in any two diametrically opposite points on the sphere. Typically, horizontal and vertical polarization are deployed. (b) Bloch sphere for TM qubits. Any two orthogonal TMs and their coherent superpositions may be used to encode TM qubits. In this example, the TMs are a zeroth and first order Hermite-Gaussian.

Quantum information encoding with TMs

Deploying TMs for quantum information encoding is an appealing prospect, because TMs can span a potentially infinite dimensional Hilbert space. This has been shown to facilitate increased information capacity per photon and increased security in quantum communication [6–8] when compared to two-dimensional encoding.

We define a *TM qudit* as a coherent superposition of d TM states:

$$|\psi\rangle_{\text{TM}}^d = \sum_{j=0}^{d-1} \alpha_j |A_j\rangle. \quad (8)$$

To highlight the formal similarity of TMs with other encoding bases, we start by discussing *TM qubits*. The most common implementation of a photonic qubit is the polarization qubit, which can be written as $|\psi\rangle = \alpha|H\rangle + \beta|V\rangle$. Here, $|H\rangle$ and $|V\rangle$ denote horizontal and vertical polarization, respectively, and $|\alpha|^2 + |\beta|^2 = 1$. Commonly, a polarization qubit is represented as a point on the surface of a Poincaré sphere as sketched in Fig. 2(a).

In analogy to this, the definition of a TM qubit requires two orthogonal states with which we associate the logical “0” and “1”. Without loss of generality, we can consider a zeroth-order and first-order Hermite-Gaussian functions of frequency to define the TMs, labeled $|\wedge\rangle$ and $|\vee\rangle$, and consequently write

$$|0\rangle \equiv |\wedge\rangle, \quad |1\rangle \equiv |\vee\rangle. \quad (9)$$

Then, a TM qubit is given by

$$|\psi\rangle_{\text{TM}} \equiv \alpha|\wedge\rangle + \beta|\vee\rangle, \quad (10)$$

where again $|\alpha|^2 + |\beta|^2 = 1$. Similar to polarization qubits, the TM qubit is best visualized as a point on the surface of a Bloch sphere as shown in Fig. 2(b).

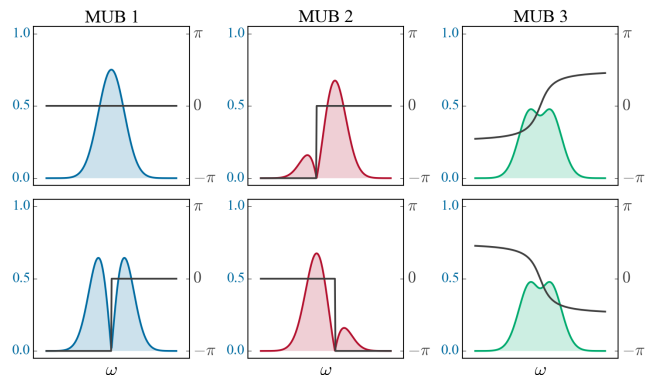


FIG. 3. The columns show the three MUBs for a TM qubit, with the fundamental TM shapes being a zeroth and first order Hermite-Gaussian, respectively. The colored areas are the spectral amplitude, whereas the dark lines are the spectral phases of the TMs, the color-coding corresponds to Fig. 2(b).

Mutually unbiased bases

Sets of bases, for which the overlap between a basis vector of one basis with any basis vector from any of the other bases has the same absolute value, are called mutually unbiased bases (MUBs) [19]. They lie at the heart of QIS applications such as quantum key distribution [20] or quantum state tomography [21]. The physical meaning of MUBs is the following: if a certain quantum state is an eigenstate of one basis then a measurement in any other MUB yields a uniformly random result yielding no information. Using polarization states, the three sets of Stokes vectors denoting horizontal and vertical, diagonal and anti-diagonal as well as left and right circular light form the typically used MUBs.

For the case of the aforementioned TM qubit from Fig. 2(b), the basis modes of the three possible MUBs are indicated by the different colors and we explicitly plot them in Fig. 3. The color coding corresponds to Fig. 2(b). If the qubit was given by $|\psi\rangle_{\text{TM}} = |\wedge\rangle$, measuring in either the red or green basis results in “0” (upper row) or “1” (lower row) with a probability of 50%.

The challenge for TMs is the implementation of a device that facilitates a mode-selective measurement, where the phase coherence plays a particularly important role. For a polarization qubit, an appropriate combination of wave plates and polarizing beam splitters readily accomplishes the projection onto the respective basis sets. For TMs, the situation is more complicated, since time-stationary operations are not sufficient for mode-selectivity and so-called quantum pulse gates have to be employed [10–13]. We return to this point below, where we briefly review the solution to the mode-sorting problem.

STATE-OF-THE-ART

TM structure of photon pair states

Today, parametric down-conversion (PDC) in optical waveguides is the workhorse for the generation of photon-pair and heralded single-photon states. Notably, PDC generates quantum states with a rich intrinsic TM structure, when ultrafast pulses are deployed as pump [22]. This structure is decoupled from the transverse spatial mode, which is solely determined by the waveguide geometry. It is encoded in the so-called joint spectral amplitude (JSA) of the PDC $f(\omega_s, \omega_i)$, which can be written as [23, 24]

$$f(\omega_s, \omega_i) = \alpha(\omega_s, \omega_i) \cdot \phi(\omega_s, \omega_i). \quad (11)$$

Here, $\alpha(\omega_s, \omega_i)$ is the pump-envelope function, which encompasses energy conservation and the spectrum of the pump pulses, and $\phi(\omega_s, \omega_i)$ is the phase-matching function, which describes momentum conservation and depends on the medium dispersion, respectively.

With that, we denote the two-photon component of the generated state

$$|\psi\rangle_{\text{PDC}} = \int d\omega_s d\omega_i f(\omega_s, \omega_i) \hat{a}^\dagger(\omega_s) \hat{b}^\dagger(\omega_i) |0, 0\rangle, \quad (12)$$

where $\hat{a}^\dagger(\omega_s)$ and $\hat{b}^\dagger(\omega_i)$ are standard monochromatic creation operators for signal and idler photons.

A decomposition of the JSA in two sets of uniquely defined TMs $\{f^{(s)}(\omega_s)\}$ and $\{f^{(i)}(\omega_i)\}$, which exhibit pairwise correlations such that

$$f(\omega_s, \omega_i) = \sum_{k=0}^{\infty} \sqrt{\lambda_k} f_k^{(s)}(\omega_s) f_k^{(i)}(\omega_i) \quad (13)$$

reveals the underlying TM structure of the PDC state [22]. Here, the expansion coefficients are normalized according to $\sum_k \lambda_k = 1$. We graphically show this expansion for a typical, non-engineered PDC in Fig. 4(a).

From Eqs. (12) and (13), we obtain

$$|\psi\rangle_{\text{PDC}} = \sum_{k=0}^{\infty} \sqrt{\lambda_k} |A_k, B_k\rangle \quad (14)$$

where we used again the broadband mode operators from Eq. (4). This expression shows that the PDC excites pairs of TMs $f_k^{(s)}(\omega_s)$ and $f_k^{(i)}(\omega_i)$ with a relative weight of $\sqrt{\lambda_k}$.

For the special case of an dispersion-engineered PDC that excites only a single pair of TMs (see, for instance [25–29]), the state from Eq. (14) reduces to $|\psi\rangle_{\text{PDC}} = |A_0, B_0\rangle$. This situation is shown in Fig. 4(b). In this case, by detecting the photon created in one channel, one heralds the single-photon state in the other channel in a known, pure TM.

Coherent manipulation of the TM structure of single-photon states

The second requirement for realizing QIS with TMs is the coherent manipulation of a state in the TM basis. This can be achieved by deploying so-called quantum pulse gates (QPGs) [10, 12, 13, 30]. Note that although we restrict our discussions to three-wave mixing implementations of QPGs here, all results can be generalized to four-wave mixing. The underlying physical process of a QPG based on three-wave mixing is dispersion-engineered sum-frequency generation (SFG) inside a nonlinear optical waveguide, where one photon from an ultrafast pump pulse and a “red” quantum signal fuse into a “green” converted output photon. Here, red and green describe two well-separated frequency bands, for instance 1535 nm (red) and 557 nm (green), respectively [11]. An adaptation of this approach for use with continuous variable quantum states has been proposed in [15]. In four-wave mixing implementations, two nondegenerate pump pulses are used, which allows smaller frequency shifts of single photons to be achieved than when using three-wave mixing [31–33].

An ideal QPG that is mode matched to the TMs of the source as defined above acts on an arbitrary single-photon input state $|\psi\rangle_{\text{in}}$ of the form Eq. 8 according to

$$|\psi\rangle_{\text{out}} = \hat{Q}_i^{(\eta)} |\psi\rangle_{\text{in}} \quad (15)$$

with

$$\begin{aligned} \hat{Q}_i^{(\eta)} = & \mathbb{1} - |A_i\rangle \langle A_i| - |C\rangle \langle C| \\ & + \cos \theta_i (|A_i\rangle \langle A_i| + |C\rangle \langle C|) \\ & + \sin \theta_i (|C\rangle \langle A_i| - |A_i\rangle \langle C|). \end{aligned} \quad (16)$$

This expression is a family of unitary transformations on the single-photon state space comprised of two non-overlapping subspaces (here, frequency bands): one spanned by the TM states $|A_j\rangle$, and a single TM state $|C\rangle$ occupying the other. It has an elegant interpretation: the QPG acts as a quantum mechanical beam splitter, which operates on TMs instead of polarization or spatial modes. As detailed below and in [30, 34], the blue pump pulse spectrum $\alpha(\omega)$ defines the targeted “red” input TM $f_i^{(s)}(\omega)$ that is selected and converted to the “green” output TM $f^{(c)}(\omega)$ with an efficiency given by $\eta = \sin^2(\theta_i)$. Note that the QPG can also select superpositions of signal TMs, when the pump pulses are shaped accordingly. The parameter θ_i describes the strength of the QPG operation and can be tuned with the pump pulse energy, although the shapes of the “red” and “green” modes will change slightly for different values of θ_i , due to time-ordering corrections [35–37] (i.e. the input and output TMs are not identical). For genuine QPG operation, $\theta_j = 0$ for $j \neq i$; that is, all TMs that are not addressed

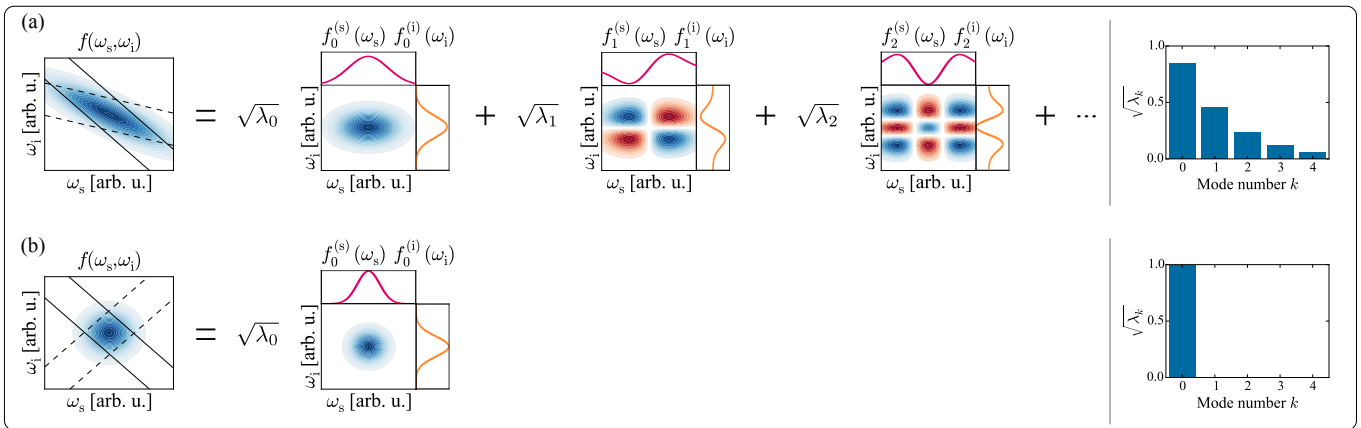


FIG. 4. (a) Representation of a general PDC process. The leftmost panel shows the JSA $f(\omega_s, \omega_i)$, which is the product of pump envelope function (black solid lines) and the phasematching function (black dashed lines). This function is decomposed into two sets of TMs $\{f^{(s)}(\omega_s)\}$ and $\{f^{(i)}(\omega_i)\}$ with weighting coefficients $\sqrt{\lambda_k}$. In the central part, we plot the first three TM pairs. The rightmost panel shows the distribution of expansion coefficients $\sqrt{\lambda_k}$. (b) A dispersion-engineered PDC process excites only one pair of TMs. The JSA does not exhibit any correlations between signal and idler photons. The distribution of weighting coefficients $\sqrt{\lambda_k}$ consequently exhibits only a single entry greater than zero.

are completely transmitted. This situation is sketched in Fig. 5(a).

From Eq. (16) we see two things. First, the QPG converts any targeted input TM $f_i^{(s)}(\omega)$ into the same output TM $f^{(c)}(\omega)$. This is important in light of large network architectures, because it facilitates interference between formerly orthogonal TMs after the QPG operation. Second, the QPG can also be operated “backwards”. In this case, it accepts one single input TM $f^{(c)}(\omega)$, which is coherently reshaped to an arbitrary output TM $f_i^{(s)}(\omega)$. This allows the treatment of the $|C\rangle$ frequency band as a buffer, or “processing” state space, and allows one to perform arbitrary linear operations on TM qudits that reside in the $\{|A_j\rangle\}$ -space using combinations of QPGs, as will be shown below.

A measure to quantify the operation fidelity of a QPG is the so-called *mode-selectivity* [12]

$$S = \frac{\sin^4(\theta_i)}{\sum_{j=0}^{\infty} \sin^2(\theta_j)} \leq 1, \quad (17)$$

which measures the ratio between the squared conversion efficiency of the selected mode and the conversion efficiencies of all modes. A mode-selectivity of 1 characterizes perfect single-TM operation, whereas a mode-selectivity of 0 signifies a total absence of modal selectivity.

It has been shown that the single-stage QPG realization from Fig. 5(a) cannot reach a mode-selectivity of $S = 1$ due to the effects of time-ordering, which lead to a temporal multimode behavior at conversion efficiencies exceeding 90% [35, 36]. This can be overcome by utilizing a two-stage Mach-Zehnder/Ramsey like setup of two successive QPGs with an efficiency of 50% each, which are driven by the same pump pulse shape [12, 13]. We sketch this in Fig. 5(b).

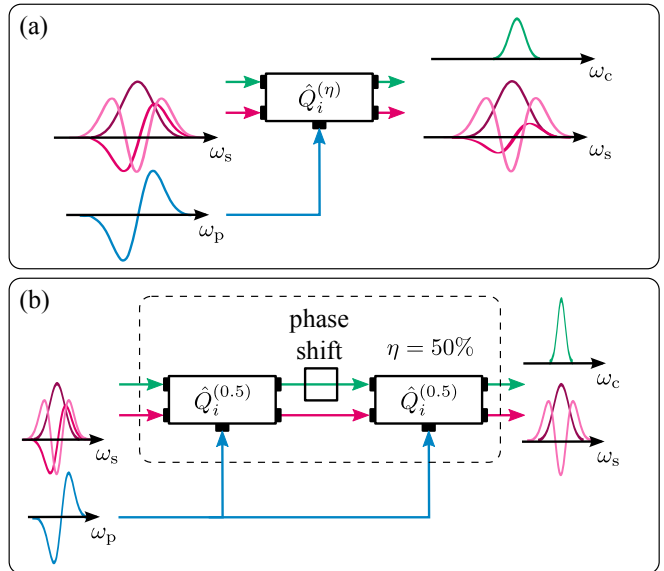


FIG. 5. (a) Schematic of the QPG operation. The shape of the blue pump pulse selects one TM from the “red” input signal and converts it to the “green” output with an efficiency of η . All other signal TMs are completely transmitted. The index i labels the addressed input TM. (b) A Mach-Zehnder/Ramsey like configuration of two successive QPGs with an efficiency of 50% each overcomes the time-ordering limitations of a single QPG and facilitates the selection and conversion of a single TM with an efficiency of 100%.

In the two-stage QPG a single photon in the target TM will be converted into an equal superposition of a “green” and a “red” mode by the first stage, and will then be coherently fully frequency shifted or back-converted in the second stage depending on an externally applied phase

shift to the device. The non-target TM components of the photon will not participate in the interferometric conversion process due to their vanishingly small per-stage conversion efficiencies, and will effectively transparently pass through the device. The need for phase coherence across the two stages can be met by deriving the two pump pulses from the same master pulse. In a specific configuration [12, 13], this method also eliminated the temporal distortion in the shapes of the “red” and “green” modes due to time-ordering effects, which enabled the cascading of QPGs without the need for inter-QPG compensatory TM reshaping. Note that the overall operation of the two QPGs is again collectively described by Eq. (16) and that we use the simplified sketch from Fig. 5(a) for reasons of convenience from here on. Various overall η values can now be achieved by tuning the interferometric phase shift inbetween the two stages (Fig. 5(b)) instead of changing the pump power. Unlike the single-stage setup, this can change the conversion efficiency of the target TM without changing its output mode shape.

In a recent experiment, the implementation of a single-stage QPG with a mode-selectivity of $S = 80\%$ at a conversion efficiency of $\eta = 87\%$ when operated at the single-photon level has been demonstrated [11].

Note that alternative approaches to TM-selective SFG are studied in [38–40], which forego group-velocity matching. Although potentially simpler from an experimental point of view, these approaches cannot generally reach high mode-selectivities as defined above [35].

COMPLETING THE TM TOOLKIT

TM engineering and TM Bell states

So far, the considerations acknowledged current state-of-the-art and were based on Gaussian pump pulses. However, in light of high-dimensional QIS based on TMs, the degree of control over the intrinsic PDC TM structure is still insufficient. Typical applications like quantum computation require at least the faithful generation of TM qubit states. In the following, we demonstrate how this can be accomplished by combining in a very natural way a dispersion-engineered PDC with pulse shaping techniques, which are well-established in the fields of ultrafast optics and coherent control (for a nice review see [41]).

To this end, we consider shaped pump pulses with Hermite-Gaussian spectra given by

$$\alpha(\omega_s, \omega_i) = \frac{1}{\sqrt{n! \sqrt{\pi} 2^n \sigma}} H_n \left(\frac{\Delta\omega}{\sigma} \right) \exp \left[-\frac{(\Delta\omega)^2}{2\sigma^2} \right]. \quad (18)$$

Here, $\Delta\omega = \omega_p - \omega_s - \omega_i$ is the frequency mismatch between the pump, signal and idler fields, $H_n(x)$ is a Hermite polynomial of order n and σ is the spectral $\frac{1}{e}$ -width

of the pump spectral intensity.

Fig. 6(a) shows an engineered PDC that is driven by a 1st order Hermite-Gaussian pump pulse. The JSA decomposes into

$$f(\omega_s, \omega_i) = \frac{1}{\sqrt{2}} \left(f_0^{(s)}(\omega_s) f_0^{(i)}(\omega_i) + f_1^{(s)}(\omega_s) f_1^{(i)}(\omega_i) \right). \quad (19)$$

This result can be interpreted such that the PDC comprises exactly two pairs of TMs with equal excitation probability. Consequently, we write the generated photon-pair state as

$$|\psi\rangle_{\text{PDC}} \approx \frac{1}{\sqrt{2}} (|A_0, B_0\rangle + |A_1, B_1\rangle) = \frac{1}{\sqrt{2}} (|\wedge_s, \wedge_i\rangle + |\vee_s, \vee_i\rangle), \quad (20)$$

where the graphical representation in the second line highlights the shapes of the individual signal and idler TMs. This state is a TM $|\psi^+\rangle$ Bell state, which is a fundamental resource for QIS applications.

In Fig. 6(b), we consider a 2nd order Hermite-Gaussian pump pulse. The decomposition of the resulting JSA shows that the generated state comprises exactly three TM pairs. Although the relative weights are not evenly distributed anymore, the dimensionality of the state is well-defined. Further increasing the order of the pump Hermite-Gaussian successively adds additional TM pairs to the structure of the generated state.

In this way it is possible to generate high-dimensional photonic states with an unprecedented degree of control. We emphasize again that all TMs “live” inside the same transverse spatial waveguide mode, which makes our approach exceptionally robust and guarantees experimental simplicity.

TM selective detection and state purification

The final requirement to render TMs a viable framework for QIS is the ability to carry out TM-selective detection, which facilitates, for instance, TM-state tomography or photon “purification”. This can be accomplished with QPGs. Let us first consider the example of “purifying” a PDC photon. We assume the general PDC state from Eq. (14) and detect one of the photons, say photon A , with a single photon detector as sketched in Fig. 7(a). This heralds photon B with a reduced density matrix that is given by

$$\hat{\rho}_B = \sum_{k=0}^{\infty} \lambda_k |B_k\rangle \langle B_k|, \quad (21)$$

which is generally a mixed state with purity $\mathcal{P} = \sum_k \lambda_k^2$.

On the other hand, we can send photon A to a QPG, which selects a single TM $f_i^{(s)}(\omega_s)$, and detect only the

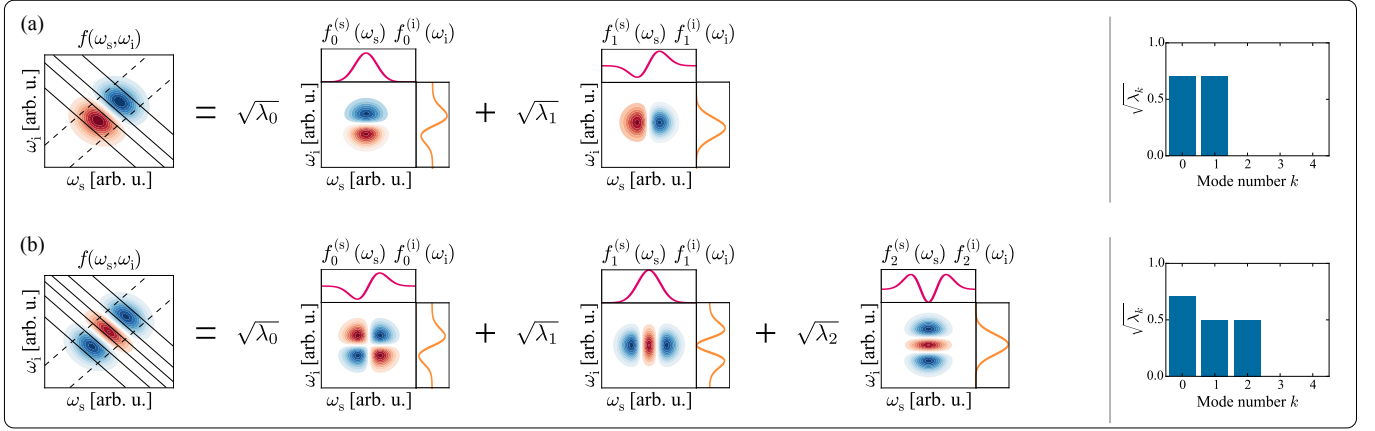


FIG. 6. (a) When pumping a dispersion engineered PDC with a 1st order Hermite-Gaussian pulse, the resulting JSA (left) has a negative part signified by the red color. Note that the pump envelope function is again denoted by solid black lines, whereas the phase-matching function is shown as dashed black lines. A decomposition of this JSA yields exactly two pairs of TMs (center) with similar expansion coefficients (right). Hence, the generated state is a TM Bell state. (b) By further increasing the order of the Hermite-Gaussian pump, it is possible to successively add TM pairs to the generated state. This state features an extremely well-defined dimensionality, although the relative weights of the modes become unbalanced.

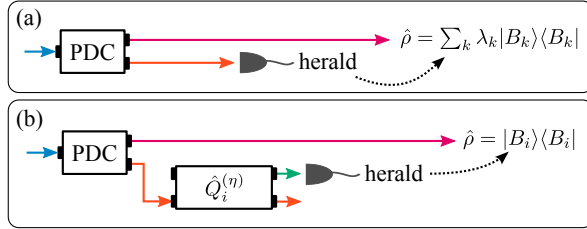


FIG. 7. (a) Non mode-selective detection of one PDC photon generally projects its sibling into a mixed state. (b) Deploying a QPG to herald a single TM yields a pure heralded broadband photon at the cost of a lowered heralding rate.

converted output. In this case, a successful detection heralds photon B , which is in a pure state with corresponding density matrix

$$\hat{\rho}_B = |B_i\rangle\langle B_i|, \quad (22)$$

as sketched in Fig. 7(b) [10]. Note that this “purification” comes at the cost of a lower heralding rate, which is reduced by the factor λ_i . This is a refinement of the classic method of heralding approximately pure-state photons by employing narrowband frequency filters in the herald-detector arm [42, 43]. The QPG acts as a complex spectral-amplitude shape “filter”, as opposed to a mere flat-band intensity filter. The spectral width (or equivalently, the temporal duration) of the target TM of the QPG can be matched to the specific properties of the PDC output to maximize heralding efficiency.

Photon TM-state tomography

Now, we turn our attention to TM quantum-state tomography. Here, the challenge is to retrieve the (complex-valued) entries of a quantum state’s density matrix in a basis of TMs. This differs from polarization-state tomography because of the higher dimensionality of the TM-state space. For an arbitrary single-photon state, the density matrix is given by

$$\hat{\rho} = \sum_{i,j} \mathcal{C}_{ij} |A_i\rangle\langle A_j|, \quad (23)$$

with associated TMs $\{f_i(\omega)\}$. This state can be analyzed with a QPG, which selects a coherent superposition of TMs given by $\zeta f_k(\omega) + \sqrt{1 - \zeta^2} e^{i\phi} f_l(\omega)$, where $\zeta \in [0, 1]$, as shown in Fig. 8(a). This function is defined by the shape of pump pulse the QPG is “programmed” with. Detecting both the converted output and the transmitted light with single photon detectors, we measure the average converted count rates R_C and R_T respectively, which are related to elements of the input density matrix by

$$\frac{R_C}{R_C + R_T} = \zeta^2 \mathcal{C}_{kk} + (1 - \zeta^2) \mathcal{C}_{ll} + 2\Re \left[\zeta \sqrt{1 - \zeta^2} e^{i\phi} \mathcal{C}_{lk} \right]. \quad (24)$$

From this expression we see that for $\zeta = 0$ and $\zeta = 1$, we directly obtain \mathcal{C}_{kk} and \mathcal{C}_{ll} , respectively. To retrieve the complex coefficient \mathcal{C}_{lk} , we set $\zeta = \frac{1}{\sqrt{2}}$ and evaluate the counts for $\phi = 0$ and $\phi = \frac{\pi}{2}$. By extension, we also obtain \mathcal{C}_{kl} and thus a complete subset of matrix coefficients of the density matrix $\hat{\rho}$. In this way, the complete density matrix or an experimentally feasible subset thereof

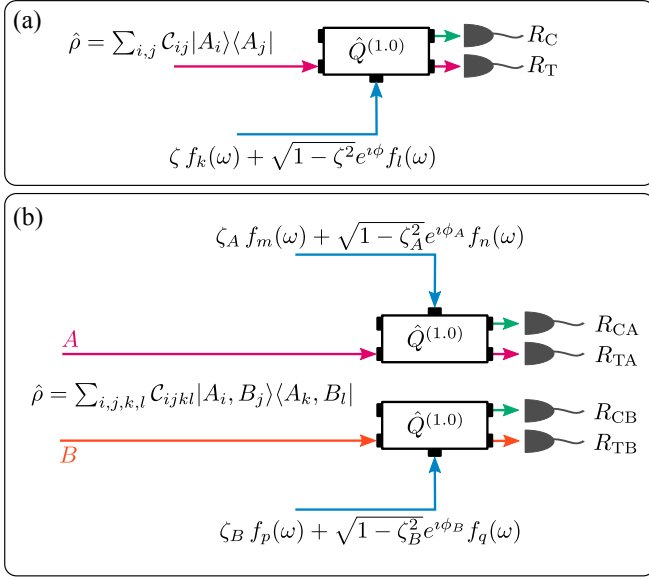


FIG. 8. (a) TM state tomography of a single-photon state with density matrix $\hat{\rho}$. Both transmitted and converted output of the QPG are detected with single-photon detectors. (b) Generalized scheme for the TM tomography of a biphoton state. Photons “1” and “2” are sent to two different QPGs and the transmitted and converted outputs are detected with single photon detectors.

can be sampled. It is important to note that any chosen portion of the density matrix can be “directly” measured

in this way without reconstructing the entire state. This is only true for QPG that can achieve unit selectivity, as without high selectivity, the elements can only be found up to an unknown normalization constant, thus necessitating the need to measure the entire matrix (or make small-magnitude assumptions about the unmeasured coefficients).

This procedure can be generalized to certain biphoton states as sketched in Fig. 8(b). A general two-photon state in two different spatial modes (with photon labels A and B) may be expressed in two sets of TM bases as

$$\hat{\rho} = \sum_{i,j,k,l} \mathcal{C}_{ijkl} |A_i, B_j\rangle \langle A_k, B_l|. \quad (25)$$

The two photons are analyzed with two separate QPGs, which select TMs given by $\zeta_A f_m(\omega) + \sqrt{1-\zeta_A^2} e^{i\phi_A} f_n(\omega)$ and $\zeta_B f_p(\omega) + \sqrt{1-\zeta_B^2} e^{i\phi_B} f_q(\omega)$, respectively. Then we employ four single-photon detectors labeled CA, TA, CB, and TB, as shown in Fig. 8(b). We can then measure coincidence rates between pairs of detectors (say between CA and CB, denoted by $R_{CA,CB}$, and so on). The following expression of such coincidence rates

$$\frac{R_{CA,CB}}{R_{CA,CB} + R_{CA,TB} + R_{TA,CB} + R_{TA,TB}} \quad (26)$$

can be expressed in terms of the biphoton density matrix elements thusly

$$\begin{aligned} & \zeta_A^2 \zeta_B^2 \mathcal{C}_{mppm} + (1-\zeta_A^2)(1-\zeta_B^2) \mathcal{C}_{nqqn} + \zeta_A^2(1-\zeta_B^2) \mathcal{C}_{mqqm} + (1-\zeta_A^2)\zeta_B^2 \mathcal{C}_{nppn} \\ & 2\Re \left[e^{i\phi_A} \zeta_A \sqrt{1-\zeta_A} (\zeta_B^2 \mathcal{C}_{mppn} + (1-\zeta_B^2) \mathcal{C}_{mqqn}) + e^{i\phi_B} \zeta_B \sqrt{1-\zeta_B} (\zeta_A^2 \mathcal{C}_{mpqm} + (1-\zeta_A^2) \mathcal{C}_{nqqn}) \right. \\ & \left. + \zeta_A \zeta_B \sqrt{1-\zeta_A} \sqrt{1-\zeta_B} (e^{i(\phi_A+\phi_B)} \mathcal{C}_{mpqn} + e^{i(\phi_A-\phi_B)} \mathcal{C}_{mqpn}) \right] \end{aligned} \quad (27)$$

Cycling through the parameter space $(\zeta_{1,2}, \phi_{1,2}) \in \{(1, -), (0, -), (\frac{1}{\sqrt{2}}, 0), (\frac{1}{\sqrt{2}}, \frac{\pi}{2})\}$ as well as varying the indices (m, n, o, p) will reveal any desired set of coefficients from the two-photon density matrix.

QIS APPLICATIONS

In this section, we detail how TMs can be utilized for both quantum communication and quantum computation exploiting the currently available technology.

Quantum communication

One important aspect of QIS is quantum communication (QC), where quantum information is transmitted

between distant parties, by convention called Alice and Bob. To this end, information has to be encoded at Alice’s location and decoded and read out at Bob’s location. Deploying the aforementioned devices and methods, a QC system based on TMs can be readily set up.

Here, we discuss two approaches to realizing this. The first approach utilizes different TMs as different communication channels and thus relies on TM multiplexing. Note that in this approach, information is not encoded in the TMs but in another degree of freedom, for instance the polarization. The second approach directly encodes the information in arbitrary superpositions of single-photon TMs, and thereby can implement genuine high-dimensional QC.

The use of TMs for channel-multiplexing would be distinguished from conventional time- or frequency-based optical multiplexing, which use either separated short

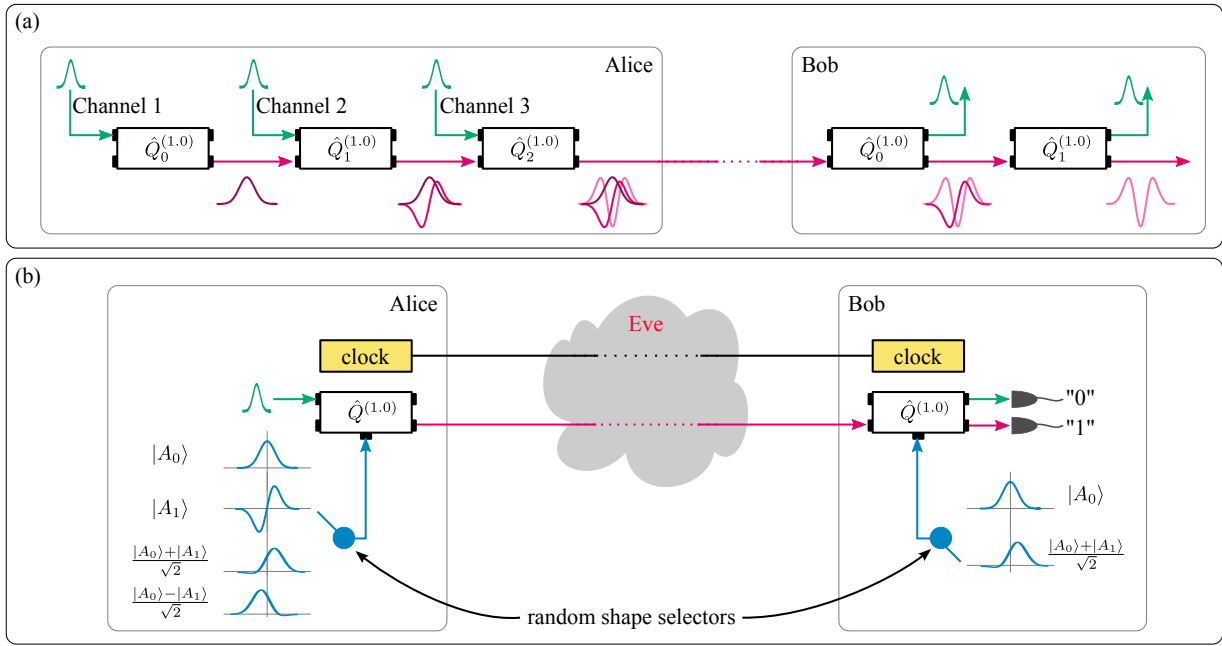


FIG. 9. Two applications of TMs to quantum communication: (a) In a TM multiplexing scenario, Alice uses orthogonal TMs as independent channels, which are sent to Bob in one single physical fiber. He de-multiplexes the channels with QPGs and reads out the information. The QPGs are being employed as TM multiplexers (Alice) and demultiplexers (Bob) on a single-mode optical channel. (b) Implementation of the BB84 QKD protocol with TMs. Alice randomly prepares one of four possible basis states and sends it to Bob, who randomly measures in one of two MUBs. The two outputs of Bobs QPG correspond to “0” and “1”. Following the original BB84 protocol, Alice and Bob can unveil the presence of an eavesdropper (Eve) by sacrificing part of the generated key.

pulses or narrow spectral windows to define different information channels. Such schemes have recently been proposed for quantum networks as well [44]. Those schemes are not based on genuinely field-orthogonal modes and thus have to rely on guard bands (empty channels) to ensure channel distinguishability. Contrary to that, TMs overlap in time and frequency, yet are field-orthogonal. Thus, they decrease the effective area in the time-frequency space that is lost to unused regions (guard bands), and thus help optimize spectral efficiency. For such a scheme to work, add/drop functionality is essential. Using the QPG, both operations can be implemented as sketched in Fig. 9(a).

On Alice’s side, a succession of QPGs adds different channels to the communication line. This is possible due to the TM-selective operation of the QPG, which reshapes the “green” input $f^{(c)}(\omega)$ into the desired “red” TM $f_i^{(s)}(\omega)$. At the same time, the existing “red” TMs $f_j^{(s)}(\omega)$ with $j \neq i$ are not affected by this operation. Note that this operation mode of the QPG has been referred to as quantum pulse shaper in an earlier publication [30]. After transmission, Bob deploys a cascade of QPGs to de-multiplex the different channels into separate ports, from which the information is read out.

The second approach, high-dimensional QC, is appealing in light of quantum key distribution (QKD) applica-

tions, where the goal is to establish a secure encryption key between Alice and Bob. Deploying TMs, the implementation of a generalized BB84 protocol [20] becomes possible. To clarify this procedure, we sketch the realization of the original BB84 protocol using two TM MUBs instead of polarization in Fig. 9(b). Alice randomly prepares one of the four possible basis states with a QPG and sends it to Bob. Bob in turn randomly chooses the measurement basis of his QPG and directly detects both output ports, which then correspond to ‘0’ and ‘1’. Thereafter, Alice and Bob publicly announce their preparation and measurement bases and keep only those events when both coincide. Sacrificing a part of the so retained key, Alice and Bob can uncover an eavesdropper by the error she introduces.

If this scheme is extended to higher-dimensional encoding, the increase in the number of MUBs can enable large-alphabet key transfer and drastically increases the error introduced by an eavesdropper, thus rendering the protocol even more secure [45–47].

Quantum computation

In this section, we discuss two implementations of quantum computation. First, we consider linear optical quantum computation (LOQC), where TM qubits prop-

agate through a linear optical network and are subject to single- and two-qubit operations, which define the computation algorithm. Then, we investigate cluster state quantum computation, where multiple TM qubits are ‘fused’ in a specific way to create a graph state with a tailored entanglement structure. Then, measurements of the nodes (photons) of the cluster state implement the computation algorithm, the result of which can be read out from the remaining nodes.

Since in this paper we focus on three-wave mixing implementations of QPGs, we are effectively restricted to one single “green” output TM $f^{(c)}(\omega)$, though we allow for a complete set of “red” input TMs $f_i^{(s)}(\omega)$. Consequently, the input TMs are treated as the primary qudit information “register” space, and the output channel will play the role of a “processing” space, in a manner similar to [48].

LOQC

In LOQC, deterministic two-qubit operations are provably impossible. However, arbitrary single qubit operations can be implemented with a combination of QPGs. For this, we require two special cases of the QPG operation from Eq. (16). First, a QPG with a conversion efficiency of 100%, and second, a QPG with a conversion efficiency of 50%. They are represented by operators

$$\hat{Q}_i^{(1,0)} = \mathbb{1} - |A_i\rangle\langle A_i| - |C\rangle\langle C| + |C\rangle\langle A_i| - |A_i\rangle\langle C|, \quad (28)$$

and

$$\begin{aligned} \hat{Q}_i^{(0,5)} &= \mathbb{1} - |A_i\rangle\langle A_i| - |C\rangle\langle C| \\ &+ \frac{1}{\sqrt{2}}(|A_i\rangle\langle A_i| + |C\rangle\langle C|) \\ &+ \frac{1}{\sqrt{2}}(|C\rangle\langle A_i| - |A_i\rangle\langle C|). \end{aligned} \quad (29)$$

In Fig. 10, we show how these operations driven by the proper pump shapes can be sequentially combined with channel-dependent phase shifts, which shift the phase only in the “green” processing space and are shown as green boxes, to implement the following single-qubit operations (up to an overall phase) on the $\{|A_0\rangle, |A_1\rangle\}$ space:

(a) Hadamard gate:

$$\hat{H} = \frac{|A_0\rangle + |A_1\rangle}{\sqrt{2}}\langle A_0| + \frac{|A_0\rangle - |A_1\rangle}{\sqrt{2}}\langle A_1| \quad (30)$$

(b) Pauli-X gate (type I, II):

$$\hat{X} = |A_1\rangle\langle A_0| + |A_0\rangle\langle A_1| \quad (31)$$

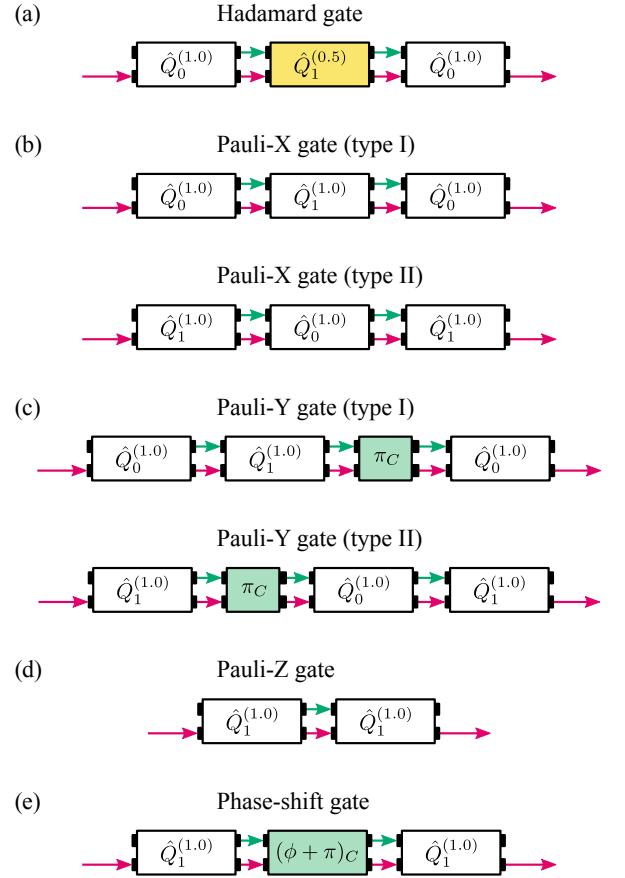


FIG. 10. Implementation of single-qubit gates for LOQC using QPGs with 100% conversion efficiency (white boxes), QPGs with 50% conversion efficiency (yellow boxes) and phase shifts of the green $|C\rangle$ TM (green boxes). Note that both the Pauli-X gate and the Pauli-Y gate have two possible experimental implementations, which differ in the order in which the red TMs $f_0^{(s)}(\omega)$ and $f_1^{(s)}(\omega)$ are addressed.

(c) Pauli-Y gate (type I, II):

$$\hat{Y} = -\iota |A_1\rangle\langle A_0| + \iota |A_0\rangle\langle A_1| \quad (32)$$

(d) Pauli-Z gate:

$$\hat{Z} = |A_0\rangle\langle A_0| - |A_1\rangle\langle A_1| \quad (33)$$

(e) Phase-shift gate:

$$\hat{\phi} = |A_0\rangle\langle A_0| + e^{i\phi} |A_1\rangle\langle A_1| \quad (34)$$

These realizations rely on only two different pump shapes, corresponding to the “red” TMs $f_0^{(s)}(\omega)$ and $f_1^{(s)}(\omega)$, which encode the logical “0” and “1”. The phase-shift gate can be simplified, if the phase $(\phi + \pi)$ is imprinted onto one of the two pump pulses. Then, the channel dependent phase shift can be omitted.

Note that the “green” channel is used only internally, whereas the input and output channels are the “red”

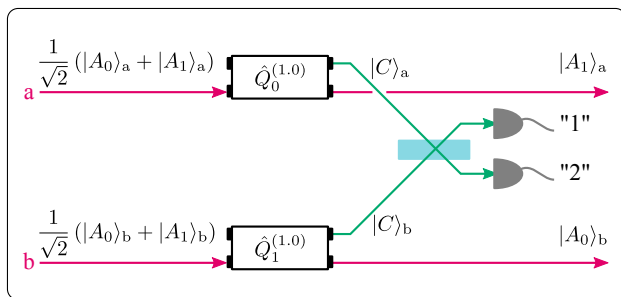


FIG. 11. Two TM qubits in spatial beams a and b can be fused with two QPGs, which select different “red” TM components from the qubits and selectively frequency-convert them. Then, the “green” outputs of the QPGs are interfered at a 50/50 beamsplitter (blue rectangle) and detected with detectors “1” and “2”. For more information, see the text.

TMs. This greatly reduces the challenge of maintaining phase relations between different frequency bands. It also eliminates the phase-coherence requirement for pump pulses across different red-channel-to-red-channel single-qubit gates, only requiring it for pump pulses internal to any given single-qubit gate. Additionally, the sequential steps can in principle be fabricated in monolithic devices, which promises a compact and robust implementation with building blocks that are well-suited to be used in integrated networks.

Cluster state quantum computation

Finally, we consider cluster state quantum computation. To efficiently grow discrete-variable cluster states from a supply of resource Bell pairs, we require several operations. Assuming that we already have a stock of linear cluster states which we want to merge into two-dimensional cluster states, we need local Hadamard transformations and projective measurements [49]. These we have already introduced in the last paragraphs. More important is the ability to generate linear cluster states from Bell pairs. In order to do so, we have to rely on qubit fusion. A practical method which facilitates this for polarization qubits has been introduced by Browne and Rudolph [50], where it was referred to as *Type-I fusion*. Here, we adapt this scheme to operate on TM qubits as defined in Eq. (10).

Two qubits in spatial beams a and b are sent to two QPGs as sketched in Fig. 11. The QPGs implement the operation $\hat{Q}_0^{(1.0)}$ on qubit a and $\hat{Q}_1^{(1.0)}$ on qubit b, respectively. This means, that the “red” TMs $f_{0,a}^{(s)}(\omega)$ and $f_{1,b}^{(s)}(\omega)$ are converted to the green TMs $f^{(c)}(\omega)_{a,b}$. The two “green” channels are interfered on a balanced beamsplitter behind the QPGs to erase any distinguishing information and the beamsplitter output ports are detected by detectors “1” and “2”. The successful de-

tection of a single “green” photon heralds the successful qubit fusion operation, which can be written in terms of Kraus operators

$$\hat{O}_{1,2} = \frac{1}{\sqrt{2}} \left(|A_0\rangle_b \langle A_0|_a \langle A_0|_b \mp |A_1\rangle_b \langle A_1|_a \langle A_1|_b \right), \quad (35)$$

where the sign depends on whether detector “1” or “2” fires. The state after a successful fusion is given by

$$|\psi\rangle_{\text{fused}} = \frac{1}{\sqrt{2}} (|A_0\rangle_b \mp |A_1\rangle_a), \quad (36)$$

which, as expected, denotes again a qubit state. Note that the two parts of the fused qubit can be deterministically combined into a single spatial mode at a polarizing beamsplitter, when the polarization of one part is rotated by 90° . In addition, the qubit fusion operation can readily be generalized to qubits that comprise two polarizations. Thus, resource-efficient generation of two-dimensional TM cluster states can be realized within our framework.

CHALLENGES

While photonic quantum-information systems are ideal for serving as intermediary between memory, interaction, and detection resources, they come with known challenges. Most notably, the absence of any direct photon-photon interaction limits all-optical quantum information processing to nondeterministic logic gates [51] or cluster-state measurement schemes [52]. When compared with optical-polarization or beam-path encoding of quantum information, the proposed TM encoding brings additional challenges, which need to be overcome in order to take advantage of the large in-principle benefits of using TMs for QIS: their relative immunity from channel dispersion and their natural compatibility with quantum memories in hybrid QIS systems, where efficient coupling into and out of disparate devices is highly dependent on temporal-mode matching. As with all burgeoning frameworks for optical QIS, the use of TMs will require significant investments in integrated device fabrication technology and timing electronics. TMs also share with other frameworks the need for efficient single-photon detection and lossless programmable optical routing.

On the other hand, TMs require heavy usage of time-dependent, active components driven by shaped laser pulses. The timing requirements may be more severe when using TMs because the TM scheme relies essentially on their temporal orthogonality, which is degraded under time jitter. To overcome this timing challenge over long-distance transmissions, we envision the use of weak coherent ‘pilot’ pulses, which when amplified at the receiver can serve as a timing reference, a pump pulse, and a transmission-medium induced linear-dispersion compensator, all in one.

The aforementioned active components are predominantly waveguides comprised of second-order or third-order nonlinear-optical materials. Monolithic chip-scale implementation of TM-photonics circuitry requires significant improvements in inter-waveguide coupling. Ultimately, TM-based schemes might have to rely on performance gains from single-mode networkability and higher dimensionality, supplemented by their accommodation of broadband quantum memories (see for instance [53]), to outperform other optical QIS frameworks.

CONCLUSION

We have shown that TMs of single photon states form an appealing framework for QIS. Formally, they are comparable with transverse spatial field modes, but have distinct advantages over spatial modes: they are naturally compatible with waveguide technology, making them ideal candidates for integration into existing communication networks, and they are not affected by typical medium distortions such as linear dispersion, which renders them robust basis states for real-world applications. Still, TMs are of yet an underused resource for QIS.

In this paper, we have shown that QIS based on TMs is feasible with current technology. We introduced a method for the generation of photon pair states, which comprise a user-defined number of TMs. This method relies on the combination of dispersion-engineered PDC with classical pulse shaping for the pump pulses of the process. Then, we discussed TM-selective detection schemes with selectivity very close to unity, which facilitate, for instance, the “purification” of PDC photons or full TM-state tomography measurements.

Thereafter, we discussed the implementation of quantum communication in the framework of TMs of single-photon states. Since different TMs are truly orthogonal, they can serve as independent communication channels in TM multiplexing scenarios. On the other hand, they can also be used to encode information into a high-dimensional state space, which opens an avenue towards high-dimensional QKD in integrated quantum network architectures. Then, we considered TM LOQC. Here, we put forward a framework for the implementation of any possible single qubit operation using only QPGs and frequency dependent phase shifts. In combination with two-photon interference, these are sufficient for universal LOQC. Finally, we demonstrated qubit fusion of TM qubits in order to generate discrete variable cluster states based on TMs, which complement the considerations on LOQC and complete a generous framework for the utilization of TMs as promising basis for QIS.

DVR and MGR were supported by the National Science Foundation through EPMD and GOALI, grant ECCS-1101811. BB and CS acknowledge financial support by the Deutsche Forschungsgemeinschaft (DFG) via

Sonderforschungsbereich TRR 142.

-
- [1] P. G. Kwiat, K. Mattle, H. Weinfurter, A. Zeilinger, A. V. Sergienko, and Y. Shih, *Phys. Rev. Lett.* **75**, 4337 (1995).
 - [2] A. Mair, A. Vaziri, G. Weihs, and A. Zeilinger, *Nature* **412**, 313 (2001).
 - [3] J. Leach, B. Jack, J. Romero, A. K. Jha, A. M. Yao, S. Franke-Arnold, D. G. Ireland, R. W. Boyd, S. M. Barnett, and M. J. Padgett, *Science* **329**, 662 (2010).
 - [4] A. C. Dada, J. Leach, G. S. Buller, M. J. Padgett, and E. Andersson, *Nature Phys.* **7**, 677 (2011).
 - [5] G. C. G. Berkhout, M. P. J. Lavery, J. Courtial, M. W. Beijersbergen, and M. J. Padgett, *Phys. Rev. Lett.* **105**, 153601 (2010).
 - [6] S. Gröblacher, T. Jennewein, A. Vaziri, G. Weihs, and A. Zeilinger, *New J. Phys.* **8**, 75 (2006).
 - [7] J. T. Barreiro, T.-C. Wei, and P. G. Kwiat, *Nature Phys.* **4**, 282 (2008).
 - [8] J. Leach, E. Bolduc, D. J. Gauthier, and R. W. Boyd, *Phys. Rev. A* **85**, 060304 (2012).
 - [9] U. M. Titulaer and R. J. Glauber, *Phys. Rev.* **145**, 1041 (1966).
 - [10] A. Eckstein, B. Brecht, and C. Silberhorn, *Opt. Express* **19**, 13770 (2011).
 - [11] B. Brecht, A. Eckstein, R. Ricken, V. Quiring, H. Suche, L. Sansoni, and C. Silberhorn, *Phys. Rev. A* **90**, 030302(R) (2014).
 - [12] D. V. Reddy, M. G. Raymer, and C. J. McKinstrie, *Opt. Lett.* **39**, 2924 (2014).
 - [13] D. V. Reddy, M. G. Raymer, and C. J. McKinstrie, *Phys. Rev. A* **91**, 012323 (2015).
 - [14] W. Sohler, D. Ostrowsky, O. Alibart, and S. Tanzilli, *Nature Photon* **8**, 109 (2013).
 - [15] V. A. Averchenko, V. Thiel, and N. Treps, *Phys. Rev. A* **89**, 063808 (2014).
 - [16] C. Simon, M. Afzelius, J. Appel, A. B. de la Giroday, S. J. Dewhurst, N. Gisin, C. Y. Hu, F. Jelezko, S. Kröll, J. H. Müller, J. Nunn, E. S. Polzik, J. G. Rarity, H. De Riedmatten, W. Rosenfeld, A. J. Shields, N. Sköld, R. M. Stevenson, R. Thew, I. A. Walmsley, M. C. Weber, H. Weinfurter, J. Wrachtrup, and R. J. Young, *Eur. Phys. J. D* **58**, 1 (2010).
 - [17] K. S. Choi, H. Deng, J. Laurat, and H. J. Kimble, *Nature* **452**, 67 (2008).
 - [18] B. J. Smith and M. G. Raymer, *New J. Phys.* **9**, 414 (2007).
 - [19] J. Schwinger, *Proc. Natl. Acad. Sci. U.S.A.* **46**, 570 (1960).
 - [20] C. H. Bennett and G. Brassard, in *Proceedings of IEEE International Conference on Computers, Systems and Signal Processing, Bangalore, India* (1984) pp. 175–179.
 - [21] D. T. Smithey, M. Beck, M. G. Raymer, and A. Faridani, *Phys. Rev. Lett.* **70**, 1244 (1993).
 - [22] C. K. Law, I. A. Walmsley, and J. H. Eberly, *Phys. Rev. Lett.* **84**, 5304 (2000).
 - [23] W. P. Grice and I. A. Walmsley, *Phys. Rev. A* **56**, 1627 (1997).
 - [24] T. E. Keller and M. H. Rubin, *Phys. Rev. A* **56**, 1534 (1997).
 - [25] A. B. U’Ren, C. Silberhorn, K. Banaszek, I. A. Walmsley,

- R. Erdmann, W. P. Grice, and M. G. Raymer, *Laser Phys.* **15**, 146 (2005).
- [26] P. J. Mosley, J. S. Lundeen, B. J. Smith, P. Wasylczyk, A. B. U'Ren, C. Silberhorn, and I. A. Walmsley, *Phys. Rev. Lett.* **100**, 133601 (2008).
- [27] O. Kuzucu, F. N. C. Wong, S. Kurimura, and S. Tovstonog, *Phys. Rev. Lett.* **101**, 153602 (2008).
- [28] X. Shi, A. Valencia, M. Hendrych, and J. P. Torres, *Opt. Lett.* **33**, 875 (2008).
- [29] A. Eckstein, A. Christ, P. J. Mosley, and C. Silberhorn, *Phys. Rev. Lett.* **106**, 013603 (2011).
- [30] B. Brecht, A. Eckstein, A. Christ, H. Suche, and C. Silberhorn, *New J. Phys.* **13**, 065029 (2011).
- [31] D. Méchin, R. Provo, J. D. Harvey, and C. J. McKinstrie, *Opt. Express* **14**, 8995 (2006).
- [32] H. J. McGuinness, M. G. Raymer, C. J. McKinstrie, and S. Radic, *IEEE Photon. Technol. Lett.* **23**, 109 (2011).
- [33] H. J. McGuinness, M. G. Raymer, C. J. McKinstrie, and S. Radic, *Phys. Rev. Lett.* **105**, 093604 (2010).
- [34] M. G. Raymer, S. J. van Enk, C. J. McKinstrie, and H. J. McGuinness, *Optics Communications* **283**, 747 (2010).
- [35] D. V. Reddy, M. G. Raymer, C. J. McKinstrie, L. Mejling, and K. Rottwitt, *Opt. Express* **21**, 13840 (2013).
- [36] A. Christ, B. Brecht, W. Mauerer, and C. Silberhorn, *New J. Phys.* **15**, 053038 (2013).
- [37] N. Quesada and J. E. Sipe, *Phys. Rev. A* **90**, 063840 (2014).
- [38] Y.-P. Huang and P. Kumar, *Opt. Lett.* **38**, 468 (2013).
- [39] A. S. Kowligy, P. Manurkar, N. V. Corzo, V. G. Velev, M. Silver, R. P. Scott, S. J. B. Yoo, P. Kumar, G. S. Kanter, and Y.-P. Huang, *Opt. Express* **22**, 27942 (2014).
- [40] J. M. Donohue, M. D. Mazurek, and K. J. Resch, *Phys. Rev. A* **91**, 033809 (2015).
- [41] A. Monmayrant, S. Weber, and B. Chatel, *J. Phys. B: At. Mol. Opt. Phys.* **43**, 103001 (2010).
- [42] H. de Riedmatten, I. Marcikic, W. Tittel, H. Zbinden, and N. Gisin, *Phys. Rev. A* **67**, 022301 (2003).
- [43] R. Kaltenbaek, B. Blauensteiner, M. Żukowski, M. Aspelmeyer, and A. Zeilinger, *Phys. Rev. Lett.* **96**, 240502 (2006).
- [44] J. Nunn, L. J. Wright, C. Söller, L. Zhang, I. A. Walmsley, and B. J. Smith, *Opt. Express* **21**, 15959 (2013).
- [45] H. Bechmann-Pasquinucci and W. Tittel, *Phys. Rev. A* **61**, 062308 (2000).
- [46] M. Bourennane, A. Karlsson, and G. Björk, *Phys. Rev. A* **64**, 012306 (2001).
- [47] N. J. Cerf, M. Bourennane, A. Karlsson, and N. Gisin, *Phys. Rev. Lett.* **88**, 127902 (2002).
- [48] P. C. Humphreys, W. S. Kolthammer, J. Nunn, M. Barbieri, A. Datta, and I. A. Walmsley, *Phys. Rev. Lett.* **113**, 130502 (2014).
- [49] G. Gilbert, M. Hamrick, and Y. S. Weinstein, *Phys. Rev. A* **73**, 064303 (2006).
- [50] D. E. Browne and T. Rudolph, *Phys. Rev. Lett.* **95**, 010501 (2005).
- [51] E. Knill, R. Laflamme, and G. J. Milburn, *Nature* **409**, 46 (2001).
- [52] R. Raussendorf and H. J. Briegel, *Phys. Rev. Lett.* **86**, 5188 (2001).
- [53] K. F. Reim, P. Michelberger, K. C. Lee, J. Nunn, N. K. Langford, and I. A. Walmsley, *Phys. Rev. Lett.* **107**, 053603 (2011).